Effect of the CuO addition on a Sb-doped SnO_2 ceramic electrode applied to the removal of Norfloxacin in chloride media by electro-oxidation

J. Carrillo-Abad[1], J. Mora-Gómez[1], M. García-Gabaldón[1], E. Ortega[1], S. Mestre[2], V. Pérez-Herranz[1],

1) IEC Group, Universitat Politècnica de València, Camí de Vera s/n, 46022, València, Spain

2) Instituto de Tecnología Cerámica, Campus Universitario Riu Sec, Av.Vicent Sos Baynat s/n, 12006, Castellón, Spain

Corresponding author: mongarga@iqn.upv.es

Abstract

Norfloxacin is employed as in veterinary and human medicine against gram-positive and gram-negative bacteria. Due to the ineffective treatment at the wastewater treatment plants it becomes an emergent pollutant. Electro-oxidation appears as an alternative to its effective mineralization. This work compares Norfloxacin electro-oxidation on different anodic materials: two ceramic electrodes (both based on SnO_2 + Sb_2O_3 with and without CuO, named as CuO and BCE, respectively) and a boron doped diamond (BDD). First, the anodes were characterized by cyclic voltammetry, revealing that NOR direct oxidation occurred at 1.30 V vs. Ag/AgCl. The higher the scan rate the higher both the current density and the anodic potential of the peak. This behavior was analyzed using the Randles–Sevcik equation to calculate the Norfloxacin diffusion coefficient in aqueous media, giving a value of D= 7.80×10^{-6} cm^2 s^{-1} at 25 °C), which is close to the predicted value obtained using the Wilke-Chang correlation.

The electrolysis experiments showed that both NOR and TOC decay increased with the applied current density, presenting a pseudo-first order kinetic. All the anodes tested achieved more

than 90% NOR degradation at each current density. The CuO is not a good alternative to BCE because although it acts as a catalyst during the first use, it is lost from the anode surface in the subsequent uses. According to their oxidizing power, the anodes employed are ordered as follows: BDD>BCE>CuO.

Keywords: Boron-doped diamond (BDD) anode, Ceramic anodes, Electro-oxidation, Norfloxacin (NOR), Voltammetric study.

1- Introduction

Norfloxacin (NOR), whose molecular structure is presented in Fig. SM-1, is widely used in veterinary and human medicine against gram-positive and gram-negative bacteria (da Silva et al., 2018; Huang et al., 2008; Mora-Gómez et al., 2019). The presence of antibiotics in the different water bodies, represents a public health risk as they not only develop and increase bacteria resistance to the antibiotic action, but also may cause specific damage to human health (Jojoa-Sierra et al., 2017; Ma et al., 2018; Mora-Gómez et al., 2019; Wohlmuth da Silva et al., 2018).

The main antibiotic discharge points into the wastewater network are pharmaceutical industries, hospitals and populated areas (Gogoi et al., 2018; Sim et al., 2011; Wohlmuth da Silva et al., 2018). This compound has a n-octanol/water distribution coefficient (log D) of -0.65 (Wang et al., 2015), so it is highly hydrophilic and its removal of wastewater presents greater difficulty compared to other compounds (Tadkaew et al., 2011). Other authors (Wells, 2006) studied this same property for different pH values, and they demonstrated that for the entire pH range the Log D of NOR was less than 1, indicating its facility of evasion from conventional methods in wastewater treatments. Consequently, NOR and other antibiotics have become emerging pollutants (EPs) as their presence has been increased up to ng L^{-1} and, in some cases, to µg L^{-1} in worldwide water bodies (Al Aukidy et al., 2012; Osorio et al., 2016; Watkinson et al., 2009; Zou et al., 2011).

Electrochemical advanced oxidation processes appear as an interesting alternative to treat these effluents. Their main advantages over other techniques are their high versatility, no addition of chemical products is needed and low energy consumption (Comninellis and Chen, 2010; Mora-Gómez et al., 2018). These technologies consist of degrading the organic compound by means of direct oxidation on the anode surface and/or the generation of strong oxidizing species. The anodes employed can be classified into two main categories: active anodes, those

57 that mainly oxidize the compound on the anode surface, and inactive anodes, which causes the
58 degradation of the organic compounds by the electrogenerated oxidizing species (Bejan et al.,
59 2012; Cañizares et al., 2004; Kapałka et al., 2009). In order to achieve the complete oxidation of
60 the organic substances the inactive anodes are more suitable than the active ones (Bejan et al.,
61 2012). There are many different inactive anodes, among which boron doped diamond (BDD) is
62 one of the most usually employed.

63 However, although BDD presents a high chemical stability, high oxygen overpotential and a wide
64 working anode potential (Comninellis and Chen, 2010; Kapałka et al., 2009), it also has several
65 drawbacks such as its high manufacture cost, which range from 8000 to 18000 € m^{-2} (Cañizares
66 et al., 2009; Sabatino et al., 2019; Soriano et al., 2019), and its own oxidation during its use. The
67 C-H groups on BDD surface may be slowly oxidized to C-OH and C=O groups, that can be further
68 oxidized to COOH and finally to CO_2. This process is studied at some works and would finally
69 cause the failure of the BDD anode (Chaplin et al., 2013, 2011; Tryk et al., 2001). Consequently,
70 new anodic materials able to avoid these drawbacks should be manufactured.

71 In this sense, the present work will study the electrochemical behaviour of ceramic electrodes
72 based on tin oxide doped with Sb_2O_3. This material is selected due to its high conductivity and
73 corrosion resistance. These low-cost electrodes have been previously tested showing good
74 results during NOR degradation in sulfate media. In these studies, the NOR degradation attained
75 using BCE varied from 85 to 100% as the applied current increased, and the BDD reached the
76 complete removal of NOR for the same experimental conditions tested. (Mora-Gómez et al.,
77 2019, 2018). However, tin oxide presents low sintering capacity, which can be improved by
78 adding sintering aids, as CuO (Mihaiu et al., 2001; Popescu et al., 2002; Zaharescu et al., 1991).
79 This work is focused on the study of the electrochemical oxidation of NOR in a common
80 electrolyte, NaCl, using three different electrodes: a commercial BDD, a ceramic electrode based

on SnO_2 doped with Sb_2O_3 (basic ceramic electrode, BCE) and another ceramic electrode with similar characteristics in which CuO is added as sintering aid (CuO).

2- Experimental

2.1- Reagents and solutions preparation

The supporting electrolytes were prepared using analytical grade reagents and distilled water. NaCl and the Norfloxacin employed to make standard solutions were purchased from Sigma-Aldrich. All the standard solutions were made using ultrapure water HPLC gradient grade from Fisher Chemical. The solutions employed at the experiments consisted of 1.64 g L^{-1} of NaCl (supporting electrolyte) in the presence or absence of 100 ppm of NOR.

2.2- Cyclic Voltammetry experiments

All these experiments were performed in a conventional three-electrode cell employing 50 mL of solution. An Ag/AgCl (saturated KCl) electrode was employed as reference electrode (RE), and all the potentials reported herein are referred to it. The counter electrode was a Pt foil with 1 cm^2 area. In the cyclic voltammetry experiments, the working electrode (WE) was one of the three different materials tested: a BDD with a 2500 ppm doping level (from NEOCOAT SA®, Switzerland) and the two new microporous SnO_2 ceramic electrodes (BCE and CuO). All the anodes presented a contact surface of 1 cm^2. The synthesis of the ceramic electrodes is well explained in previous works (Mora-Gómez et al., 2019, 2018). They are manufactured using SnO_2 as main component (purity 99.85%, Quimialmel® S.A., Spain), Sb_2O_3 as a dopant (purity 99%, Alfa-Aesar®, Germany), and CuO (when present) as a sintering aid (purity 97%, Panreac® S.A., Spain). Their composition is summarized in Table SM-1, at supplementary information.

The cyclic voltammetry, CV, experiments were carried out using a computer controlled by an Autolab PGSTAT302N (Methrom) potentiostat/galvanostat. Previously to each CV, the WE was polarized at 2 V vs. Ag/AgCl for 30 s in order to clean the anode surface and assure the complete oxidation of the metal oxides present at the ceramic electrodes. The scan rate ranged from 10 to 100 mV s^{-1}. The initial potential was the open circuit potential, and polarization was first applied in the positive direction within an upper and lower potential limit of 3 and -1 V vs. Ag/AgCl. All the cyclic voltammetry experiments were carried out at room temperature.

2.3- Electrolysis experiments

The electrochemical reactor was a Pyrex glass of 250 cm^3 filled with a 100 ppm of NOR in 1.64 g L^{-1} of NaCl. All the experiments were performed under stirring conditions. The cathode was an AISI 304 stainless steel sheet of 20 cm^2 while the RE was the same aforementioned. Regarding the anode, the same electrode materials as those employed at the CV experiments were tested. All the anodes were submerged in the solution in order to obtain a contact surface of 5.28 cm^2.

Electro-oxidation experiments were carried out under galvanostatic conditions at three different current densities (76, 114, 189 mA cm^{-2}) by the use of a power supply. The electrode potential, cell voltage and current were recorded during the electrolysis while samples were taken from the reactor each 30 min. From these samples, the NOR degradation was calculated by the measure of its absorbance wavelength at 275 nm using an Unicam UV4-200 UV/vis spectrometer. The NOR mineralization was followed by both the total organic carbon (TOC) and the inorganic ions (NH_4^+, NO_3^- and F^-) using a Shimadzu TNM-L ROHS TOC analyser and a Metrohm Ionic Chromatograph 883 Basic IC Plus, respectively. All the experiments were performed at room temperature for 4 h.

The mineralization current efficiency, was determined as follows (Guinea et al., 2010):

$$MCE = \frac{nFV\Delta(TOC)_t}{7.2\times10^5 mIt} \quad (1)$$

where n is the number of electrons transferred in the mineralization process (90), F is the Faraday constant, V is the volume of the reactor (in L), I is the applied current (A), $\Delta(TOC)_t$ is the removed organic carbon (mg L^{-1}) at a given time, m is the number of C atoms in a NOR molecule (16) and 7.2×10^5 is the conversion factor for the units homogenization (60 s min^{-1} × 12000 mg mol^{-1}). n was assumed as 90 supposing the complete mineralization of NOR according to reaction (2). This assumption was corroborated experimentally as shown at the results and discussion section, and was also observed by da Silva et al (da Silva et al., 2018):

$$C_{16}H_{18}FN_3O_3 + 38\ H_2O \rightarrow 16\ CO_2 + 3\ NO_3^- + F^- + 94\ H^+ + 90\ e^- \quad (2)$$

3- Results and discussion

3.1- Voltammetric analysis

Fig. 1a presents the cyclic voltammetry obtained for a solution containing just the supporting electrolyte (NaCl) and both NaCl and NOR for all the electrodes under study. Comparing the supporting electrolytes CVs of the BDD and the BCE anodes, the electrochemical window is wider for the BDD anode (2.05 V vs. Ag/AgCl) than for the BCE (1.85 V vs. Ag/AgCl for the BDD) as expected (Lobato et al., 2005; Panizza et al., 2008; Polcaro et al., 2006). The supporting electrolyte voltammogram obtained for the CuO anode practically overlaps the one obtained for the BCE (not shown).

When the CVs obtained in presence of NOR for the different electrode materials are compared with those obtained with only the supporting electrolyte, Fig. 1a, an anodic peak at 1.30 V vs. Ag/AgCl is observed, which only appears in the presence of NOR in solution, and is in concordance with the results of da Silva et al. (da Silva et al., 2018). Although other authors place the NOR oxidation peak between 0.9 and 1.1 V vs. Ag/AgCl (da Silva et al., 2015; Devaraj et al., 2013; Goyal et al., 2012; Huang et al., 2008; Liu et al., 2018), this difference in the peak potential can be associated to the variation of the different working conditions such as, the supporting electrolyte, NOR concentration, pH and, specially, electrode material, etc. since these works use electrodes as sensors. Additionally, another anodic wave at 1.7 V vs. Ag/AgCl is also detected. This can be related to the contribution of two processes: the oxidation of an intermediate compound generated during NOR oxidation (Coledam et al., 2016; da Silva et al., 2018) together with the onset of the oxygen electrochemical reaction.

From Fig. 1b, which represents the effect of scan rate on the CVs, it is clearly observed that the NOR oxidation peak increases and shifts to more anodic potentials as the scan rate increases and, additionally, it does not show a reversal peak which is a typical behaviour of an electrochemical irreversible process (Nicholson and Shain, 1964). This fact, which was also

observed by other authors working in NOR detection (da Silva et al., 2015; Devaraj et al., 2013; Goyal et al., 2012; Huang et al., 2008; Liu et al., 2018), is commonly observed in the electro-oxidation of organic compounds (Carrillo-Abad et al., 2018).

In order to determine the limiting step of the direct oxidation of NOR, its current peak intensity (I_p) was plotted as a function of the square root of the scan rate ($v^{1/2}$), Fig. 1c. The I_p values showed a linear trend with $v^{1/2}$, indicating the presence of a diffusion-controlled oxidation process. Nevertheless, the linear fitting does not intercept the origin, which is related to an additional process other than diffusion (García-Gabaldón et al., 2011; Trejo et al., 1998) taking place during the NOR direct oxidation on the anode surface. This process is probably associated with the adsorption of a NOR oxidation product on the anode surface, which also explains the absence of a NOR reduction counter peak at Fig. 1b (Aoki and Chen, 2016).

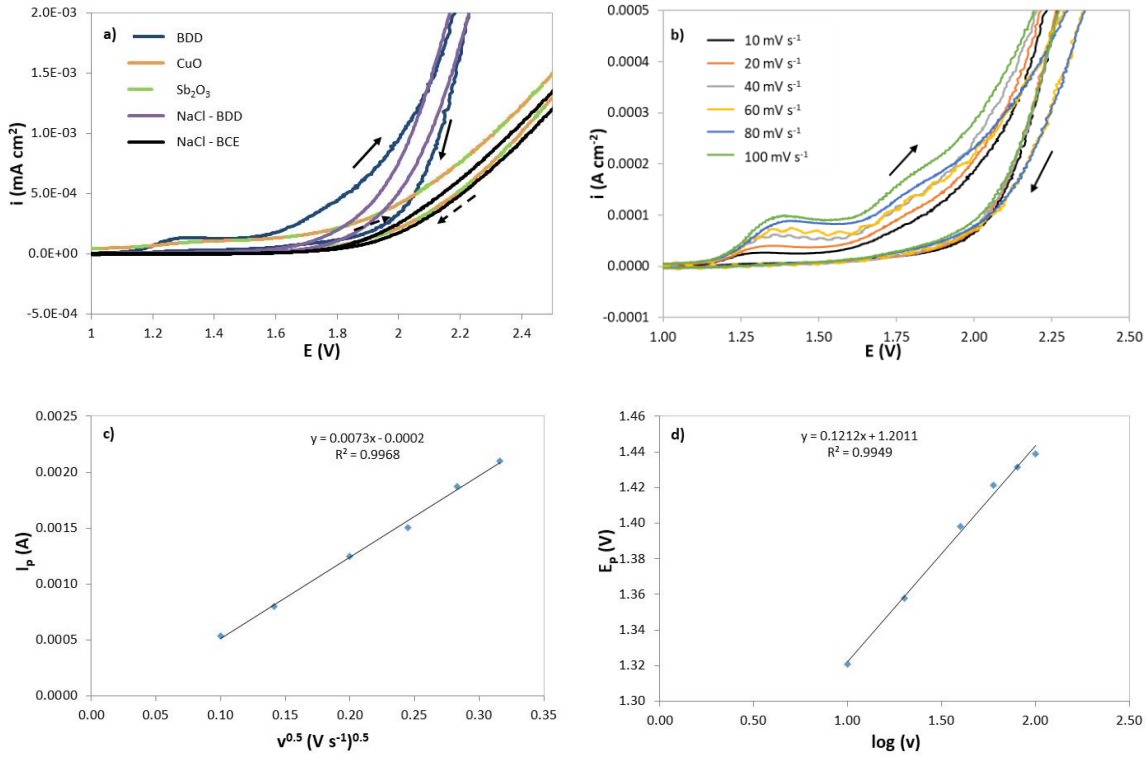

Fig. 1: Voltammetric study of NOR in a NaCl solution: a) anodic response as a function of the electrode material at 10 mV s^{-1}, b) CV zoom at NOR peak for BDD at different scan rates, c)

peak current as a function of the square root of the scan rate and, d) peak potential variation with the scan rate logarithm. Anodes surface = 1 cm^2, $[NOR]_0$= 100 ppm, $[NaCl]_0$= 1.64 g L^{-1}

The relationship between I_p and v for an irreversible process can be studied by the Randles-Sevick equation:

$$I_p = 0.496\, nFCAD^{\frac{1}{2}} \left(\frac{(\alpha \cdot n_\alpha) Fv}{RT}\right)^{\frac{1}{2}} \quad (3)$$

where A is the electrode area in cm^2, D is the diffusion coefficient of the oxidized species in cm^2 s^{-1}, C is the NOR concentration in mol cm^{-3}, v is the scan rate in V s^{-1}, F is the Faraday constant in C, R is the gas constant in J mol^{-1} K^{-1}, T is the absolute temperature in K and n is the number of transferred electrons which is assumed as 2 according to the mechanism suggested for the NOR oxidation in previous works (Devaraj et al., 2013; Liu et al., 2018) and is shown at supplementary information (Fig. SM-2). Otherwise, Fig. 1d represents the increase of E_p with the logarithm scan rate, displaying a linear relationship that permits the $\alpha \cdot n_\alpha$ determination by the Laviron's theory (Laviron, 1979). On the basis of the previous discussion a $\alpha \cdot n_\alpha$ of 0.489 is determined.

Therefore, the NOR diffusion coefficient in aqueous media was calculated using the linear fitting of the experimental data presented in Fig. 1c and the Randles-Sevick equation, giving a value of 7.80×10^{-6} cm^2 s^{-1}. This result is very similar to that calculated by the semi-empirical Wilke-Chang correlation (7.26×10^{-6} cm^2 s^{-1}), which is generally employed to estimate this parameter for organic compounds in aqueous media (Perry and Green, 2008). The Wilke-Chang correlation (Wilke and Chang, 1955) together with the values employed for its determination is shown at the Supplementary information (as Eq. SM1).

3.2- Effect of current density

Figs. 2a-c show the evolution of the NOR decay profile with time for all the applied current densities using the electrochemical reactor of 250 cm^3 with the different electrodes under study. Although the first increase in the current density (from 76 to 114 mA cm^{-2}) caused a growth in the degradation rate, this growth did not appear when the highest current was applied. This fact together with the exponential trend showed in all the figures is characteristic of a process under mass transport control (Urtiaga et al., 2018). It is worth to note that in both ceramic electrodes a maximum 90% NOR degradation is observed.

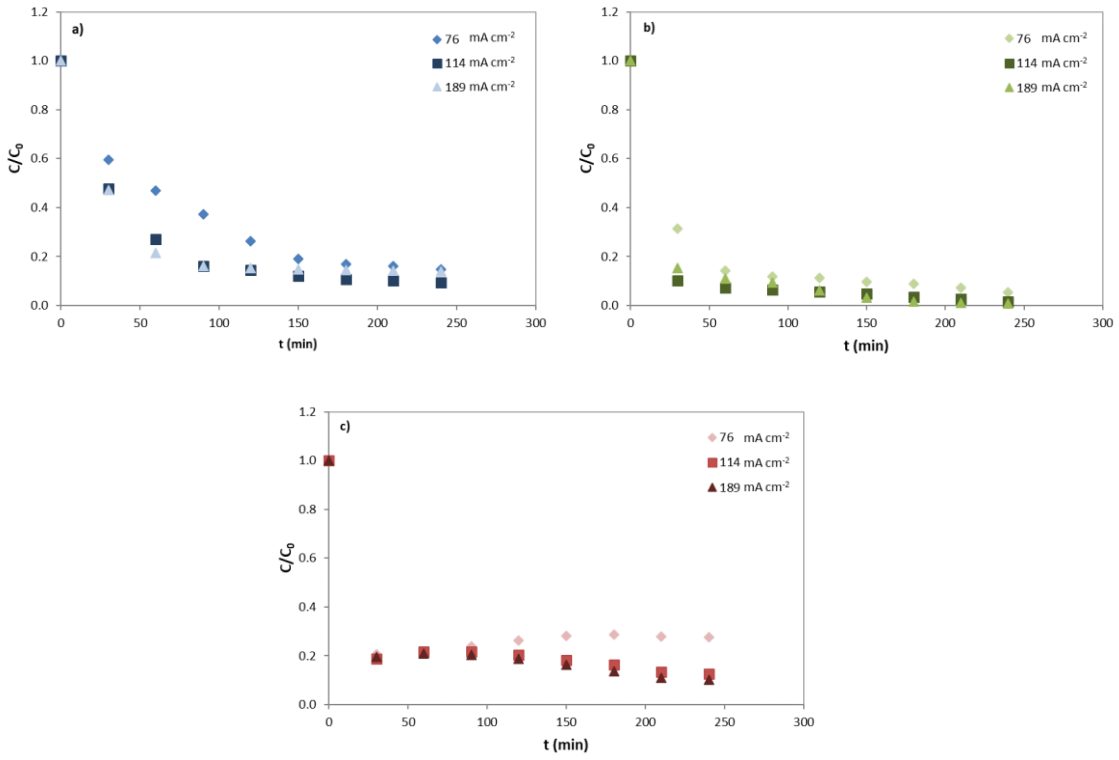

Fig. 2: C/C_0 decay profile for all the currents density applied for the different anode materials: a) CuO, b) BDD and c) BCE . $[NOR]_0$= 100 ppm, $[NaCl]_0$=1.64 g L^{-1}

A deeper sigh into the UV diagram (Figs. 3a and 3b) for these electrodes show a change in the main peak, which is related to the intermediate degradation compounds, that modify the values obtained at λ= 276 nm, causing the misreading of the values for NOR concentration. Concerning the evolution of the UV-visible spectra, previously to the electrolysis start, the same spectrum is obtained for all the electrodes tested. Two main peaks are observed for the original sample, one at 276 nm and another at 330 nm, which are associated with the aromatic ring absorption and the electronic transition of the quinolones nitrogen atom from n → ∏* (HOMO-LUMO) respectively (Neugebauer et al., 2005). Once the electrolysis began, both peaks decreased, which indicates the NOR degradation. However, the spectrum significantly changes from one electrode to another. While the quinolone group absorption remained during the first electrolysis time for both CuO and BDD (Figs. 3a and 3b) electrodes, it completely disappeared when the BCE was used (Fig. 3b). Furthermore, the main peak (276 nm) was displaced to higher wavelengths during the BCE experiment (Fig. 3c) while it was moved to lower λ values for the CuO and BDD electrodes (Figs. 3a and 3b). These differences can be attributed to the generation of by products with less substituent for the CuO and BDD electrodes, while intermediates with a more chromophore substituent were generated when the BCE was used (Woodward, 1942a, 1942b, 1941; Woodward and Clifford, 1941). Therefore, two different degradation mechanisms may be expected as function of the electrode material used. On the other hand, a new absorption peak between 200 and 220 nm appears in all the electrolysis performed, which is related to the generation of short chain carboxylic acids (Coledam et al., 2016; Mora-Gómez et al., 2019) as corroborated in the ionic analysis section.

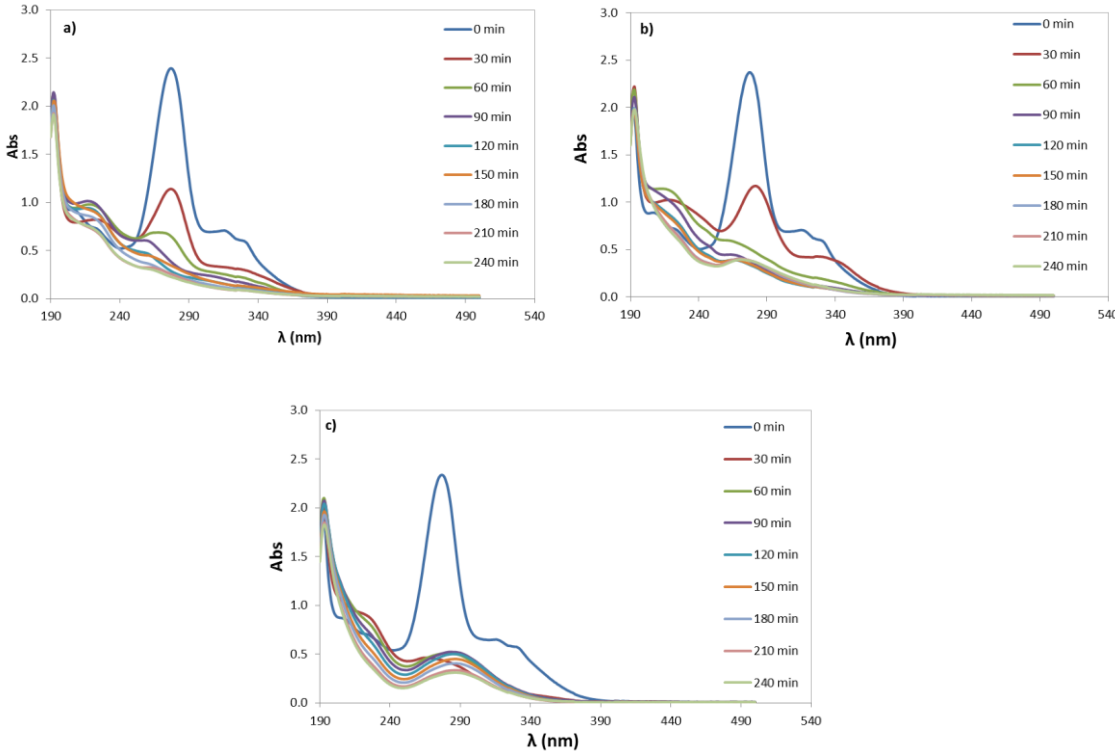

Fig. 3: UV-vis spectrum at the sampling times for the different anode materials: a) CuO, b) BDD and c) BCE. These spectra where obtained at 114 mA cm^{-2} in all cases. $[NOR]_0$= 100 ppm, $[NaCl]_0$= 1.64 g L^{-1}

Regarding TOC decay evolution with time for all the applied current densities and electrodes (Figs. 4a-c), the higher the applied current density the higher the velocity of NOR mineralization for all the anodes studied, which is related to the higher amount of oxidizing species generated during the electrolysis at higher values of applied current (Diban, 2018; Pipi et al., 2014) that also contribute to the NOR mineralization.

From the comparison of Figs. 4a-c it in inferred that the higher mineralization degree is obtained for the BDD, followed by the BCE and, finally, using the CuO anode. At the lowest applied current density the results obtained with the BDD and the BCE are very similar but as the applied density current increases, the differences between the mineralization rates obtained by using both anodes also increase. This can be attributed to the higher oxidising power of BDD anodes, since

the it has a higher oxygen overpotential, and presents a weaker hydroxyl radical adsorption than the ceramic one (Chen et al., 2005; Mora-Gómez et al., 2019).

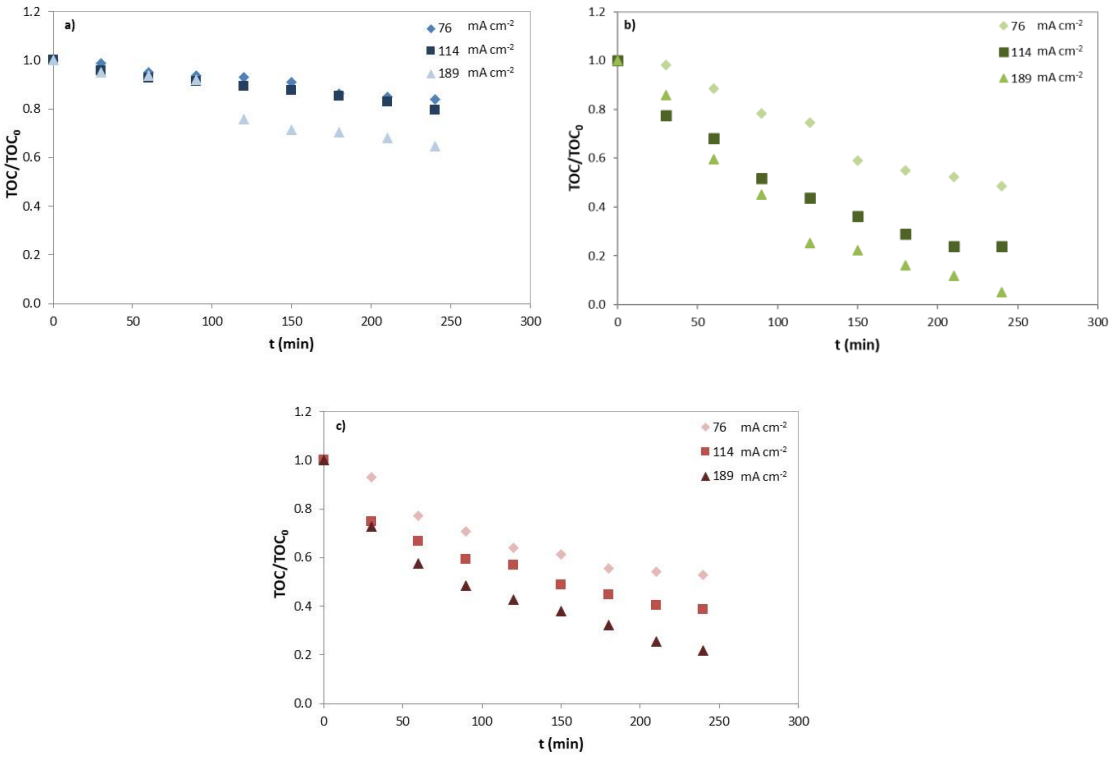

Fig. 4: TOC/TOC_0 decay profile for all the currents density applied for the different anode materials: a) CuO, b) BDD and c) BCE. $[NOR]_0$= 100 ppm, $[NaCl]_0$= 1.64 g L^{-1}

The mineralization current efficiency (Fig. SM-3) showed a common behaviour for all the anodes under study. For any applied current, the MCE decreases with time, which is characteristic of a process under mass transfer control. Nevertheless, MCE decreases with the highest applied current density due to the higher amount of energy wasted in parallel reactions together with the generation of an excess of oxidants that reacts among them. The results obtained for the BCE are very similar to those obtained by the BDD anode (not shown).

3.2- Effect of anode material

Table 1 summarizes the apparent kinetic constants for NOR removal as a function of the anode material for all the applied current densities, which are calculated from Fig. 2 assuming a pseudo-first order kinetics reaction for NOR electro-oxidation. The higher the applied current the higher the apparent kinetic constant. This fact may be related to the higher generation of oxidizing species as the applied current increases.

Table 1: Apparent first order kinetic constant values (min^{-1}) for NOR degradation at each anode tested as a function of the applied current density. $[NOR]_0$= 100 ppm, $[NaCl]_0$= 1.64 g L^{-1}

i(mA cm^{-2})	**CuO**	**BDD**	**BCE**
76	0.0105	0.0337	0.026
114	0.036 first use	0.0421	0.0315
	0.021		
189	0.0222	0.0502	0.0318

From Table 1, it is inferred that NOR electro-oxidation is faster on the BDD than in the ceramic anodes, and that the basic ceramic anode (BCE) presents higher values than those obtained for the CuO, except when this latter is used for the first time. It is also noticeable that CuO electrode presents a considerable different oxidizing power from its first use in relation to the following ones as can be seen in Figs. SM-4a and SM-4b at supplementary information. The oxidizing power of the CuO electrode during its first use is comparable to that obtained using the BDD anode (Figs. 2b and 4b) because the CuO present at the anode is dissolved into the solution acting as a catalyst for the oxidation of the organic compounds. This catalytic behaviour of Cu^{+2} has also been observed by other authors during the oxidation of phenolic compounds (Gözmen et al., 2003; Santos et al., 2002).

281 The presence of copper in solution has been experimentally confirmed by atomic absorption
282 spectroscopy. During the successive uses of this anode, the results are getting worse, reaching
283 lower TOC values than those obtained using the basic ceramic electrode of SnO_2 (BCE) as
284 observed in Fig. 4. This is due to the fact that when the electrode loses the Cu^{+2} of the surface,
285 its composition becomes similar to that of the BCE. The lower active surface of the CuO electrode
286 in relation to the BCE is responsible for this mechanism, since the copper electrode is denser
287 (apparent density of 6.696 g cm^{-3}) than the BCE (apparent density of 3.3533 g cm^{-3}).

288 Summarizing the data obtained previously in terms of degree of mineralization and degradation,
289 it is concluded that the BDD presents the best percentages of both parameters, and the CuO
290 does not represent a good alternative to the basic ceramic anode as the loss of copper worsens
291 its behaviour. Although the ceramic electrodes presented lower values of NOR removal than the
292 BDD, the values obtained are similar or higher than those obtained by another anodes also
293 formed by metallic oxides, as observed in the Table presented at the supplementary material
294 (Table SM-2), where the comparison of the NOR removal rate obtained using different anodic
295 material is presented.

296

297 *3.3- Ionic analysis*

298 The generation of fluoride, together with nitrogen ionic compounds and short-chain organic
299 acids are expected from NOR oxidation. In addition, the chloride ions provided by the supporting
300 electrolyte were also measured as they can be oxidized to some active species, which may also
301 be involved in NOR oxidation.

302 Concerning the main nitrogen ionic compound generated during NOR electro-oxidation, a high
303 controversy exists since some authors present the ammonium as main compound (Mora-Gómez
304 et al., 2019; Özcan et al., 2016), while others only detects NO_3^- (da Silva et al., 2018). In the

present work, nitrite and nitrate ions were detected, while any ammonium was observed in any experiment. This fact may be related to the presence of chlorine oxidizing species that can oxidize ammonium to both nitrite and nitrate ions.

Regarding the organic ions detected (supplementary Fig. SM-5), they ranged from the small ones (formate, acetate and oxalate ions), medium sized (such as tartrate ions) and aromatic (like phthalate ions). For BDD and BCE, Figs. SM-5b and SM-5c, initially, the organic ions detected were mainly the aromatic, although the BDD presented significant formate and acetate ions from the very beginning. As the electrolysis drew on, phthalate ions disappeared while tartrate and oxalate increased but they became the main organic ions only for a discrete instant as formate and acetate concentrations continuously grown up to become the main organic ions detected. On the other hand, the CuO anode, Fig. SM-5a presented a high amounts of phthalate and tartrate for the whole electrolysis time, maybe due to its lower oxidation power, while in terms of oxalate, formiate and acetate, it showed a similar behaviour to that observed for the other materials tested.

Fig. 5 presents the denitrogenation (dN) and defluorination (dF) from NOR, dechlorideation (dCl) from electrolyte and the % of TOC measured associated with the organic ions measured for all the materials tested at 114 mA cm^{-2}. Each of these parameters increased, independently of the anodic material, as the experiment drew on due to both NOR and NaCl oxidation. However, these rates are directly related to the oxidizing power discussed above, that is, the BDD presents the higher dCl rate, almost a 90%, associated with the higher generation of oxidative species, which helps to obtain gretarer dN and dF rates. Additionally, BDD also shows the higher amount of TOC related to the acid organic ions, achieving more than the 85% of the removal of the remaining TOC. After the BDD, the BCE anode presents good values as dN, dF and the TOC removal related with organic acids reached a 70% which is a significant value considering that the dCl rate only achieved a 50%. It is worth to note that the CuO anode showed the lowest

values but it is also remarkable that dN, dF and the TOC removal from organic acids are close to the 50% while the dCl rate is close to the 15%.

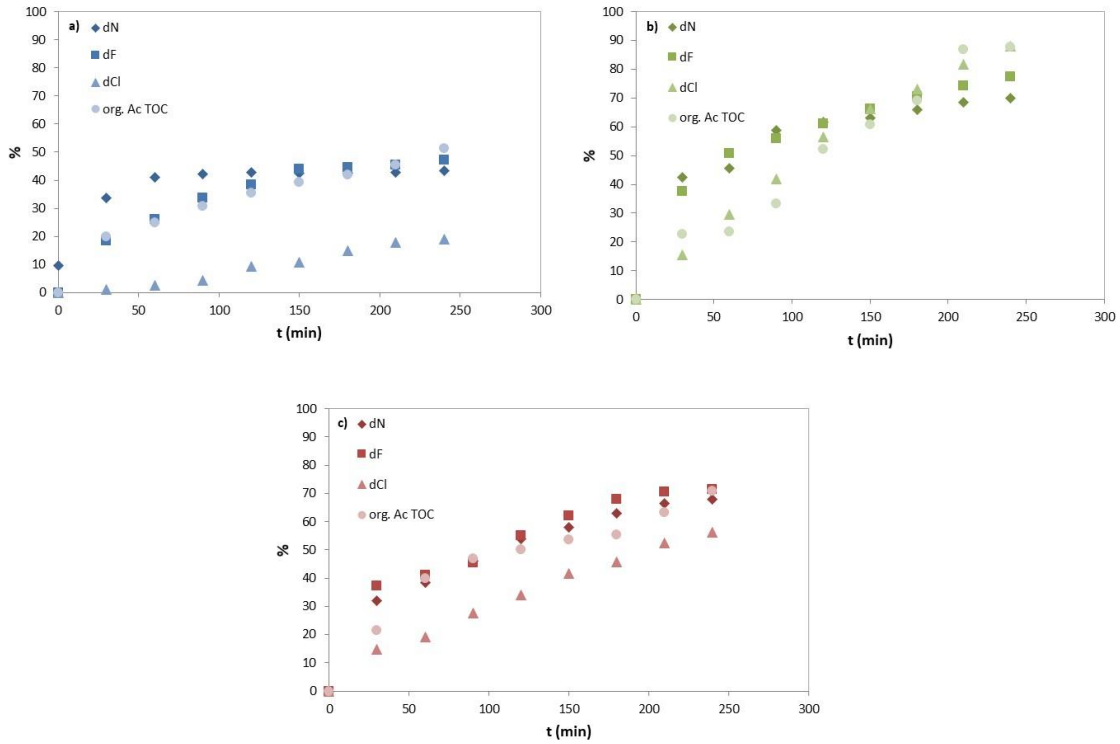

Fig. 5: Defluorination, denitrogenation, dechlorination and fractional TOC of organic acid ions profile for all the anodic materials tested: a) CuO, b) BDD and c) BCE. $[NOR]_0$= 100 ppm. $[NaCl]_0$= 1.64g L^{-1} and i= 114 mA cm^{-2}

4- Conclusions

This work is focused on the study of the electrochemical oxidation of NOR in a common electrolyte, NaCl, using three different electrodes: a commercial BDD, a ceramic electrode based on SnO_2 doped with Sb_2O_3 (basic ceramic electrode, BCE) and another ceramic electrode with similar characteristics in which CuO is added as sintering aid (CuO).

From the voltammetric analysis obtained for the different electrode materials an anodic peak at 1.30 V vs. Ag/AgCl was observed, which was attributed to NOR oxidation. Additionally, another anodic wave at 1.7 V vs. Ag/AgCl was also detected, related to the contribution of two processes: the oxidation of an intermediate compound generated during NOR oxidation together with the onset of the oxygen electrochemical reaction. NOR oxidation was classified as an irreversible process and controlled not only by diffusion. The diffusion coefficient for NOR in aqueous media was calculated as 7.80×10^{-6} $cm^2\ s^{-1}$ at 25 °C.

The higher mineralization and degradation degrees were obtained for the BDD, followed by the BCE and, finally, using the CuO anode. The apparent kinetic constants for NOR removal assuming a pseudo-first order kinetics reaction were calculated as a function of the anode material, presenting the following tendency: BDD>BCE>CuO. The CuO electrode presented a considerable different oxidizing power from its first use in relation to the following ones because the copper present at the anode is dissolved into the solution acting as a catalyst for the oxidation of the organic compounds. After this process, although the composition of the CuO anode becomes similar to that of the BCE, its lower active surface worsens the process.

From the results obtained in this study, it is inferred that the BDD presents the best results. The CuO does not represent a good alternative to the basic ceramic anode as the loss of copper worsens its behaviour. Although the ceramic electrodes presented lower values of NOR removal than the BDD, the values obtained are similar or higher than those obtained by other anodes also formed by metallic oxides.

Acknowledgments

The authors want to express their gratitude to the Ministerio de Economía y Competitividad (Spain) and the FEDER funds, which financially support the projects CTQ2015-65202-C2-1-R, CTQ2015-65202-C2-2-R and RTI2018-101341-B-C21.

371 **References**

372 Al Aukidy, M., Verlicchi, P., Jelic, A., Petrovic, M., Barcelò, D., 2012. Monitoring release of
373 pharmaceutical compounds: Occurrence and environmental risk assessment of two WWTP
374 effluents and their receiving bodies in the Po Valley, Italy. Sci. Total Environ. 438, 15–25.
375 https://doi.org/10.1016/J.SCITOTENV.2012.08.061

376 Aoki, K.J., Chen, J., 2016. Tips of Voltammetry, in: Intech. p. 19.
377 https://doi.org/http://dx.doi.org/10.5772/57353

378 Bejan, D., Guinea, E., Bunce, N.J., 2012. On the nature of the hydroxyl radicals produced at
379 boron-doped diamond and Ebonex® anodes. Electrochim. Acta 69, 275–281.
380 https://doi.org/10.1016/j.electacta.2012.02.097

381 Cañizares, P., García-Gómez, J., Lobato, J., A. Rodrigo, M., 2004. Modeling of Wastewater
382 Electro-oxidation Processes Part I. General Description and Application to Inactive
383 Electrodes. Ind. Eng. Chem. Res. 43, 1915–1922. https://doi.org/10.1021/ie0341294

384 Cañizares, P., Paz, R., Sáez, C., Rodrigo, M.A., 2009. Costs of the electrochemical oxidation of
385 wastewaters: A comparison with ozonation and Fenton oxidation processes. J. Environ.
386 Manage. 90, 410–420. https://doi.org/10.1016/j.jenvman.2007.10.010

387 Carrillo-Abad, J., Pérez-Herranz, V., Urtiaga, A., 2018. Electrochemical oxidation of 6:2
388 fluorotelomer sulfonic acid (6:2 FTSA) on BDD: electrode characterization and mechanistic
389 investigation. J. Appl. Electrochem. 48, 589–596. https://doi.org/10.1007/s10800-018-
390 1180-8

391 Chaplin, B.P., Hubler, D.K., Farrell, J., 2013. Understanding anodic wear at boron doped diamond
392 film electrodes. Electrochim. Acta 89, 122–131.
393 https://doi.org/10.1016/j.electacta.2012.10.166

Chaplin, B.P., Wyle, I., Zeng, H., Carlisle, J.A., Farrell, J., 2011. Characterization of the performance and failure mechanisms of boron-doped ultrananocrystalline diamond electrodes. J. Appl. Electrochem. 41, 1329–1340. https://doi.org/10.1007/s10800-011-0351-7

Chen, X., Gao, F., Chen, G., 2005. Comparison of Ti/BDD and Ti/SnO_2-Sb_2O_5 electrodes for pollutant oxidation. J. Appl. Electrochem. 35, 185–191. https://doi.org/10.1007/s10800-004-6068-0

Coledam, D.A.C., Aquino, J.M., Silva, B.F., Silva, A.J., Rocha-Filho, R.C., 2016. Electrochemical mineralization of norfloxacin using distinct boron-doped diamond anodes in a filter-press reactor, with investigations of toxicity and oxidation by-products. Electrochim. Acta 213, 856–864. https://doi.org/10.1016/j.electacta.2016.08.003

Comninellis, C., Chen, G., 2010. Electrochemistry for the Environment. Springer, New York.

da Silva, H., Pacheco, J., Silva, J., Viswanathan, S., Delerue-Matos, C., 2015. Molecularly imprinted sensor for voltammetric detection of norfloxacin. Sensors Actuators B Chem. 219, 301–307. https://doi.org/10.1016/J.SNB.2015.04.125

da Silva, S.W., Ortega, E.M., Rodrigues, M.A.S., Bernardes, A.M., Pérez-Herranz, V., 2018. The role of the anode material and water matrix in the electrochemical oxidation of norfloxacin. Chemosphere 210, 615–623. https://doi.org/10.1016/j.chemosphere.2018.07.057

Devaraj, M., Deivasigamani, R.K., Jeyadevan, S., 2013. Enhancement of the electrochemical behavior of CuO nanoleaves on MWCNTs/GC composite film modified electrode for determination of norfloxacin. Colloids Surfaces B Biointerfaces 102, 554–561. https://doi.org/10.1016/J.COLSURFB.2012.08.051

417 Diban, N., 2018. Electrochemical mineralization and detoxification of naphthenic acids on boron-
418 doped diamond anodes.

419 García-Gabaldón, M., Carrillo-Abad, J., Ortega-Navarro, E., Pérez-Herranz, V., 2011.
420 Electrochemical study of a simulated spent pickling solution. Int. J. Electrochem. Sci. 6,
421 506–519.

422 Gogoi, A., Mazumder, P., Tyagi, V.K., Tushara Chaminda, G.G., An, A.K., Kumar, M., 2018.
423 Occurrence and fate of emerging contaminants in water environment: A review. Groundw.
424 Sustain. Dev. 6, 169–180. https://doi.org/10.1016/j.gsd.2017.12.009

425 Goyal, R.N., Rana, A.R.S., Chasta, H., 2012. Electrochemical sensor for the sensitive
426 determination of norfloxacin in human urine and pharmaceuticals. Bioelectrochemistry 83,
427 46–51. https://doi.org/10.1016/J.BIOELECHEM.2011.08.006

428 Gözmen, B., Oturan, M.A., Oturan, N., Erbatur, O., 2003. Indirect electrochemical treatment of
429 bisphenol A in water via electrochemically generated Fenton's reagent. Environ. Sci.
430 Technol. 37, 3716–3723. https://doi.org/10.1021/es034011e

431 Guinea, E., Garrido, J.A., Rodríguez, R.M., Cabot, P.-L., Arias, C., Centellas, F., Brillas, E., 2010.
432 Degradation of the fluoroquinolone enrofloxacin by electrochemical advanced oxidation
433 processes based on hydrogen peroxide electrogeneration. Electrochim. Acta 55, 2101–
434 2115. https://doi.org/10.1016/j.electacta.2009.11.040

435 Huang, K.-J., Liu, X., Xie, W.-Z., Yuan, H.-X., 2008. Electrochemical behavior and voltammetric
436 determination of norfloxacin at glassy carbon electrode modified with multi walled carbon
437 nanotubes/Nafion. Colloids Surf. B. Biointerfaces 64, 269–74.
438 https://doi.org/10.1016/j.colsurfb.2008.02.003

439 Jojoa-Sierra, S.D., Silva-Agredo, J., Herrera-Calderon, E., Torres-Palma, R.A., 2017. Elimination of

the antibiotic norfloxacin in municipal wastewater, urine and seawater by electrochemical oxidation on IrO_2 anodes. Sci. Total Environ. 575, 1228–1238. https://doi.org/10.1016/J.SCITOTENV.2016.09.201

Kapałka, A., Fóti, G., Comninellis, C., 2009. The importance of electrode material in environmental electrochemistry Formation and reactivity of free hydroxyl radicals on boron-doped diamond electrodes. Electrochim. Acta 54, 2018–2023. https://doi.org/10.1016/j.electacta.2008.06.045

Laviron, E., 1979. General expression of the linear potential sweep voltammogram in the case of diffusionless electrochemical systems. J. Electroanal. Chem. Interfacial Electrochem. 101, 19–28. https://doi.org/10.1016/S0022-0728(79)80075-3

Liu, Z., Jin, M., Cao, J., Wang, J., Wang, X., Zhou, G., van den Berg, A., Shui, L., 2018. High-sensitive electrochemical sensor for determination of Norfloxacin and its metabolism using MWCNT-CPE/pRGO-ANSA/Au. Sensors Actuators B Chem. 257, 1065–1075. https://doi.org/10.1016/J.SNB.2017.11.052

Lobato, J., Paz, R., Rodrigo, M.A., Saez, C., 2005. Electrochemical oxidation of phenolic wastes with boron-doped diamond anodes 39, 2687–2703. https://doi.org/10.1016/j.watres.2005.04.042

Ma, X., Cheng, Y., Ge, Y., Wu, H., Li, Q., Gao, N., Deng, J., 2018. Ultrasound-enhanced nanosized zero-valent copper activation of hydrogen peroxide for the degradation of norfloxacin. Ultrason. Sonochem. 40, 763–772. https://doi.org/10.1016/j.ultsonch.2017.08.025

Mihaiu, S., Scarlat, O., Aldica, G., Zaharescu, M., 2001. SnO_2 electroceramics with various additives. J. Eur. Ceram. Soc. 21, 1801–1804. https://doi.org/10.1016/S0955-2219(01)00119-4

463 Mora-Gómez, J., García-Gabaldón, M., Ortega, E., Sánchez-Rivera, M.-J., Mestre, S., Pérez-
464 Herranz, V., 2018. Evaluation of new ceramic electrodes based on Sb-doped SnO_2 for the
465 removal of emerging compounds present in wastewater. Ceram. Int. 44, 2216–2222.
466 https://doi.org/10.1016/J.CERAMINT.2017.10.178

467 Mora-Gómez, J., Ortega, E., Mestre, S., Pérez-Herranz, V., García-Gabaldón, M., 2019.
468 Electrochemical degradation of norfloxacin using BDD and new Sb-doped SnO_2 ceramic
469 anodes in an electrochemical reactor in the presence and absence of a cation-exchange
470 membrane. Sep. Purif. Technol. 208, 68–75.
471 https://doi.org/10.1016/J.SEPPUR.2018.05.017

472 Neugebauer, U., Szeghalmi, A., Schmitt, M., Kiefer, W., Popp, J., Holzgrabe, U., 2005. Vibrational
473 spectroscopic characterization of fluoroquinolones. Spectrochim. Acta Part A Mol. Biomol.
474 Spectrosc. 61, 1505–1517. https://doi.org/10.1016/J.SAA.2004.11.014

475 Nicholson, R.S., Shain, I., 1964. Theory of Stationary Electrode Polarography. Single Scan and
476 Cyclic Methods Applied to Reversible, Irreversible, and Kinetic Systems. Anal. Chem. 36,
477 706–723.

478 Osorio, V., Larrañaga, A., Aceña, J., Pérez, S., Barceló, D., 2016. Concentration and risk of
479 pharmaceuticals in freshwater systems are related to the population density and the
480 livestock units in Iberian Rivers. Sci. Total Environ. 540, 267–277.
481 https://doi.org/10.1016/j.scitotenv.2015.06.143

482 Özcan, A., Atılır Özcan, A., Demirci, Y., 2016. Evaluation of mineralization kinetics and pathway
483 of norfloxacin removal from water by electro-Fenton treatment. Chem. Eng. J. 304, 518–
484 526. https://doi.org/10.1016/j.cej.2016.06.105

485 Panizza, M., Kapalka, A., Comninellis, C., 2008. Oxidation of organic pollutants on BDD anodes
486 using modulated current electrolysis 53, 2289–2295.

https://doi.org/10.1016/j.electacta.2007.09.044

Perry, R.H., Green, D.W., 2008. Perry's Chemical Engineers' Handbook, The effects of brief mindfulness intervention on acute pain experience: An examination of individual difference. https://doi.org/10.1017/CBO9781107415324.004

Pipi, A.R.F., Sirés, I., De Andrade, A.R., Brillas, E., 2014. Application of electrochemical advanced oxidation processes to the mineralization of the herbicide diuron. Chemosphere 109, 49–55. https://doi.org/10.1016/j.chemosphere.2014.03.006

Polcaro, A.M., Ricci, P.C., Palmas, S., Ferrara, F., Anedda, A., 2006. Characterization of boron doped diamond electrodes during oxidation processes: Relationship between electrochemical activity and ageing time. Thin Solid Films 515, 2073–2078. https://doi.org/10.1016/j.tsf.2006.06.033

Popescu, A., Mihaiu, S., Zuca, S., 2002. Microstructure and Electrochemical Behaviour of some SnO_2-based Inert Electrodes in Aluminium Electrolysis. Zeitschrift für Naturforsch. A 57a, 71–75. https://doi.org/10.1515/zna-2002-9-1010

Sabatino, S., Galia, A., Saracco, G., Scialdone, O., 2019. Development of an Electrochemical Process for the Simultaneous Treatment of Wastewater and the Conversion of Carbon Dioxide to Higher Value Product. ChemElectroChem IV, 150–159. https://doi.org/10.1002/celc.201600475

Santos, A., Yustos, P., Quintanilla, A., Rodríguez, S., García-Ochoa, F., 2002. Route of the catalytic oxidation of phenol in aqueous phase. Appl. Catal. B Environ. 39, 97–113. https://doi.org/10.1016/S0926-3373(02)00087-5

Sim, W.-J., Lee, J.-W., Lee, E.-S., Shin, S.-K., Hwang, S.-R., Oh, J.-E., 2011. Occurrence and distribution of pharmaceuticals in wastewater from households, livestock farms, hospitals

and pharmaceutical manufactures. Chemosphere 82, 179–86. https://doi.org/10.1016/j.chemosphere.2010.10.026

Soriano, Á., Gorri, D., Biegler, L.T., Urtiaga, A., 2019. An optimization model for the treatment of perfluorocarboxylic acids considering membrane preconcentration and BDD electrooxidation. Water Res. 164. https://doi.org/10.1016/j.watres.2019.114954

Tadkaew, N., Hai, F.I., McDonald, J.A., Khan, S.J., Nghiem, L.D., 2011. Removal of trace organics by MBR treatment: The role of molecular properties. Water Res. 45, 2439–2451. https://doi.org/10.1016/j.watres.2011.01.023

Trejo, G., Ortega, R., Meas, Y., Ozil, P., Chainet, E., Nguyen, B., 1998. Nucleation and Growth of Zinc from Chloride Concentrated Solutions. J. Electrochem. Soc. 145, 4090–4097.

Tryk, D.A., Tsunozaki, K., Rao, T.N., Fujishima, A., 2001. Relationships between surface character and electrochemical processes on diamond electrodes: Dual roles of surface termination and near-surface hydrogen. Diam. Relat. Mater. 10, 1804–1809. https://doi.org/10.1016/S0925-9635(01)00453-8

Urtiaga, A., Soriano, A., Carrillo-Abad, J., 2018. BDD anodic treatment of 6:2 fluorotelomer sulfonate (6:2 FTSA). Evaluation of operating variables and by-product formation. Chemosphere 201. https://doi.org/10.1016/j.chemosphere.2018.03.027

Wang, X. mao, Li, B., Zhang, T., Li, X. yan, 2015. Performance of nanofiltration membrane in rejecting trace organic compounds: Experiment and model prediction. Desalination 370, 7–16. https://doi.org/10.1016/j.desal.2015.05.010

Watkinson, A.J.J., Murby, E.J.J., Kolpin, D.W.W., Costanzo, S.D.D., 2009. The occurrence of antibiotics in an urban watershed: from wastewater to drinking water. Sci. Total Environ. 407, 2711–23. https://doi.org/10.1016/j.scitotenv.2008.11.059

533 Wells, M.J.M., 2006. Log DOW: Key to understanding and regulating wastewater-derived
534 contaminants. Environ. Chem. 3, 439–449. https://doi.org/10.1071/EN06045

535 Wilke, C.R., Chang, P., 1955. Correlation of diffusion coefficients in dilute solutions. AIChE J. 1,
536 264–270. https://doi.org/10.1002/aic.690010222

537 Wohlmuth da Silva, S., Arenhart Heberle, A.N., Pereira Santos, A., Siqueira Rodrigues, M.A.,
538 Pérez-Herranz, V., Moura Bernardes, A., 2018. Antibiotics mineralization by
539 electrochemical and UV-based hybrid processes: evaluation of the synergistic effect.
540 Environ. Technol. (United Kingdom) 3330, 1–11.
541 https://doi.org/10.1080/09593330.2018.1478453

542 Woodward, R.B., 1942a. Structure and Absorption Spectra. III. Normal Conjugated Dienes. J. Am.
543 Chem. Soc. 64, 72–75. https://doi.org/10.1021/ja01253a018

544 Woodward, R.B., 1942b. Structure and absorption spectra. IV. Further observations on a,b-
545 unsaturated ketones. J. Am. Chem. Soc. 64, 76–77. https://doi.org/doi:
546 10.1021/ja01253a019

547 Woodward, R.B., 1941. Structure and the Absorption Spectra of α,β-Unsaturated Ketones. J. Am.
548 Chem. Soc. 63, 1123–1126. https://doi.org/10.1021/ja01849a066

549 Woodward, R.B., Clifford, A.F., 1941. Structure and Absorption Spectra. II. 3-Acetoxy-Δ5-(6)-nor-
550 cholestene-7-carboxylic Acid. J. Am. Chem. Soc. 63, 2727–2729.
551 https://doi.org/10.1021/ja01855a063

552 Zaharescu, M., Mihaiu, S., Zuca, S., Matiasovsky, K., 1991. Contribution to the study of SnO_2-
553 based ceramics. Part I High-temperature interactions of tin (IV) oxide with antimony (III)
554 oxide and copper (II) oxide. Jorunal Mater. Sci. 26, 1666–1672.

555 Zou, S., Xu, W., Zhang, R., Tang, J., Chen, Y., Zhang, G., 2011. Occurrence and distribution of

556 antibiotics in coastal water of the Bohai Bay, China: impacts of river discharge and
557 aquaculture activities. Environ. Pollut. 159, 2913–20.
558 https://doi.org/10.1016/j.envpol.2011.04.037

559